

Biological endpoints as candidates for induction in bystander cells

From among the wide array of biological endpoints studied in bystander cells, there are two broad categories; measurements of pro- or anti-carcinogenic changes in cells, or, measurements of the induction or receipt of an intercellular signal (with some overlap between the two). The former are typically endpoints of cell death, cell survival, colony formation, proliferation rates, DNA damage or mutation; the latter, include cytokine secretion/activation, protein expression, calcium flux and the generation of reactive oxidative species. The aim of this project was not only to detect any effects in unirradiated bystander cells, but to assess the carcinogenic potential of any such changes. As such, the three endpoints chosen for analysis in this study were cell death via apoptosis, proliferation and chromosomal damage (detected as protein expression from an inverted transgenic reporter sequence). These three represent those endpoints most significant to the alteration of cancer risk and the most commonly analysed biological outcomes in published bystander data.

Apoptosis

Ionising radiation-induced DNA damage can result in complex, irreparable lesions that cause cells to switch from pro-survival to apoptosis pathways (Bree *et al.*, 2004). Apoptosis after ionising radiation exposure has been considered the response of cells unable to repair DNA damage sites correctly (Meng *et al.*, 1998; Radford, 2002b; Belyaev, 2005). The most critical DNA lesions, double-strand breaks, can be produced either from direct energy deposition or during attempted repair or replication at other damaged sites (reviewed in Kaina, 2003). The requirement of complex DNA damage for triggering apoptosis can be seen by treatment with clastogens producing either single- or double-strand breaks (Mekid *et al.*, 2003), or

DNA incorporation of high- or low-LET radionuclides that produce different types of DNA damage (Radford, 2002a). Radiation-sensitive cell lines require a similar number of high-LET disintegrations but far fewer low-LET decays to induce apoptosis, suggesting that repairable non-lethal damage can become lethal when repair is deficient (Meng *et al.*, 1998; Radford, 2002a).

However, radiation-induced apoptosis not linked to DNA damage has also been described. Cells surviving high-dose irradiation that are cultured for 60–80 generations show a persistent increased incidence of apoptosis along with markers of long-term oxidative stress (Limoli *et al.*, 1998; Mendonca *et al.*, 2005). Numerous studies have shown the parallel involvement of radiation-induced DNA damage and activation of cell membrane and nuclear sphingomyelinases to produce ceramide, resulting in the activation of the mitochondrial apoptosis pathway (Jaffrezou *et al.*, 2001; Kolesnick and Fuks, 2003). Protecting against radiation-induced apoptosis using scavengers of oxidative species in the mitochondria has demonstrated the interlinking of the radiation-induced DNA damage and apoptosis pathways (Lee *et al.*, 2005b). Apoptosis can also be induced by extracellular signalling, through membrane-bound receptors (Itoh *et al.*, 1991; reviewed in Thorburn, 2004) or direct chemical interactions within the cell (Langer *et al.*, 1996; Messmer and Brune, 1996a; Heigold *et al.*, 2002; Portess *et al.*, 2007). The induction of apoptosis in bystander cells observed *in vitro* could occur through any or all of these pathways.

Choice of assay

A variety of techniques is available for the detection of apoptotic cells *in situ*. These techniques each exploit hallmark features characteristic of the progressive stages of apoptotic cell death: caspase activation, chromatin cleavage and nuclear

morphological changes. Among the methods available, the terminal transferase-mediated dUTP nick end-labelling (TUNEL) technique has been the most widely used for *in situ* detection of apoptosis (Pulkkänen *et al.*, 2000; Garrity *et al.*, 2003; Kelly *et al.*, 2003).

The TUNEL method exploits the 3'-hydroxyl termini that remain on DNA fragments during the ordered chromatin cleavage that occurs during the later stages of apoptosis. Labelled nucleotides can be incorporated at the 3'-OH ends, and then visualised using direct or indirect methods. Recent methods which use nucleotides conjugated with fluorescein isothiocyanate (FITC) allow visualisation of labelled cells without the need for a chromogenic or antibody-mediated developing step.

Non-specific staining while using the TUNEL reaction has been reported in a small number of circumstances:

- due to post-mortem DNA damage occurring before fixation or during over- or under-fixation (Garrity *et al.*, 2003);
- due to DNA damage resulting from antigen-unmasking using protease in paraffin embedded tissues (Garrity *et al.*, 2003);
- due to necrotic, endonuclease-mediated DNA strand-breaks in cells produced after oncotic cell death (Grasl-Kraupp *et al.*, 1995; Kelly *et al.*, 2003); and,
- in specific cell-types i.e. proximal, distal and collecting tubular cells in mouse kidney (Pulkkänen *et al.*, 2000).

However, in conjunction with careful tissue preparation, optimisation of the labelling protocol and the use of appropriate controls, the TUNEL method remains the most widely used and trusted method for *in situ* apoptosis labelling (Schreurs *et al.*, 1997; Garrity *et al.*, 2003; Kelly *et al.*, 2003). Specifically, the use of frozen tissues allows for rapid and controlled fixation of the thin cross-sections and removes the need for antigen unmasking. The non-specific TUNEL staining reported in certain cell-types in mice, was not observed in the spleen tissues of the same animals (Pulkkänen *et al.*, 2000). As for the distinction between apoptotic and oncotic cell death, a detailed study of the specificity of the TUNEL reaction showed that the specificity was related to the type of tissue injury applied and that cells which were detected as non-specifically stained showed evidence of post-apoptotic secondary necrosis (Kelly *et al.*, 2003). The authors suggest that confusion between oncotic cell death and secondary necrotic changes in apoptotic cells (clearly distinguished by the apoptotic nuclear morphology) may be responsible for reports of poor specificity.

Apoptotic cells within the recipient spleen frozen tissue sections were identified using a commercial kit (*In situ Cell Death Detection Kit- Fluorescein*, Roche Applied Science, IN, USA) applying a modified protocol. Adaptations were applied to the manufacturer's supplied protocol based on the work of (Schreurs *et al.*, 1997), which detailed improvements to provide optimal results in frozen mouse tissues. Optimisation of TUNEL staining methods to each particular application has been suggested as an essential step in producing accurate results; but that once optimised, a standardised protocol can reliably produce consistent results (Garrity *et al.*, 2003).

Method:

Frozen tissues were brought from ultra-cold storage up to -18°C prior to sectioning. Non-serial $5\ \mu\text{m}$ -thick sections were cut from the frozen embedded tissue blocks using a *Reichert-Jung Cryocut 1800* cryostat (Leica Microsystems GmbH, Wetzlar, Germany) and applied to positively-charged glass microscope slides. Slides were allowed to dry at room temperature overnight before fixation for 30 min in 1% formaldehyde (from paraformaldehyde in PBS) according to the method of Schreurs *et al.* (1997). Slides were washed 3×10 min in PBS to remove fixative before immersion in a permeabilisation solution of 1% Triton® X-100 and 1% sodium citrate (w/v) in PBS for 10 min at room temperature before washing 3×5 min in PBS. *TUNEL reaction mixture* (*In situ* Cell Death Detection Kit) was prepared as per manufacturer's instructions and kept on ice. The fixed tissue sections were ringed with a hydrophobic barrier pen (*PAP Pen*, Zymed Laboratories Inc, CA, USA) before adding $50\ \mu\text{L}$ of *TUNEL reaction mixture* to each section. Negative controls were incubated instead with *TUNEL reaction mixture* omitting the *TdT enzyme solution* (non-specific fluorescence control). Positive controls were incubated for 10 min with 325 units of deoxyribonuclease I (Sigma Aldrich Corp.) to completely digest the DNA prior to the TUNEL reaction. The slides were incubated for 1 h at 37°C in a humidified chamber before washing 3×5 min in PBS. Slides were coverslipped with *Vectashield® with DAPI* and stored in the dark at -20°C .

Scoring method

Apoptotic cells were scored by manually counting TUNEL-positive cells in pseudo-coloured photographs overlaying the DAPI/nuclear counterstain (blue), fluorescein/TUNEL staining (green) and CMRA/donor cell fluorescent probe (red) (*Figure 4.24*).

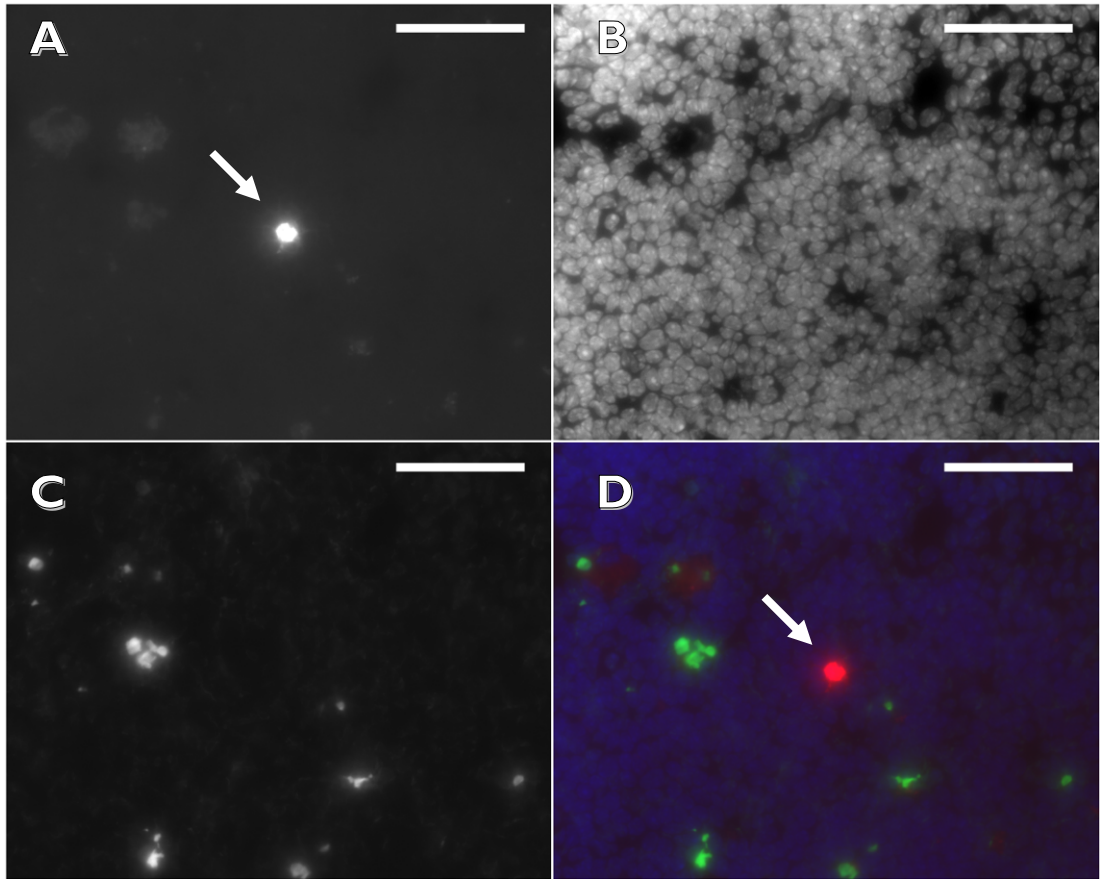


Figure 4.24: Pseudo-coloured overlay of a local screening field from TUNEL-stained spleen section

Spleen sections from recipient mice were stained for the TUNEL assay as described. Using fluorescence microscopy, lodged donor cells were identified using the filterset for CMRA fluorescence (A) and the field of view was centred on the donor cell (arrowed). In the same field, cell nuclei counterstained with DAPI (B) and fluorescent TUNEL-staining (C) were photographed. The images from the three fluorescent channels, CMRA (red), DAPI (blue), and TUNEL (green), were overlayed to form a pseudo-coloured composite image for manual screening (D) centred on the donor cell (arrowed). Scale bars show 50 μm .

Cells were scored as apoptotic when:

- their nucleus exhibited strong fluorescein fluorescence that co-localised with the DAPI nuclear counterstaining;
- the nucleus showed signs of condensation, blebbing or fragmentation;
- the cell was not fluorescently labelled on the CMRA channel; and,
- the object did not show signs of non-specific fluorescence on the CMRA channel.

When fragmentation of an apoptotic nucleus (common in apoptotic cells) resulted in several distinct small particles (*Figure 4.25*) or when a TUNEL-positive nucleus was already ingested by a phagocytic cell (*Figure 4.26*), the nucleus was scored as a single event. The apoptosis frequency was calculated for each field as the quotient of the number of TUNEL-positive cells (*Figure 4.27*) and the estimated number of recipient splenocytes in the field (*Figure 4.28*), for both local and global fields. The apoptosis frequency was calculated for each spleen section as the mean frequency across each of the fields photographed, and for each mouse as the unweighted mean of the duplicate slides as recommended by Garrity *et al.* (2003).

A manual scoring method counting the number of TUNEL-positive cells was chosen over the use of automatic measurement of the total TUNEL-stained area as studies have shown that the manual counting method shows a better correlation with semi-quantitative assessment of apoptosis and less variability between duplicate sections than area measurements (Garrity *et al.*, 2003). The discrepancy between the two methods is thought to arise from changes in nuclear size associated with apoptosis that make ratios of TUNEL staining to total cell area inconsistent.

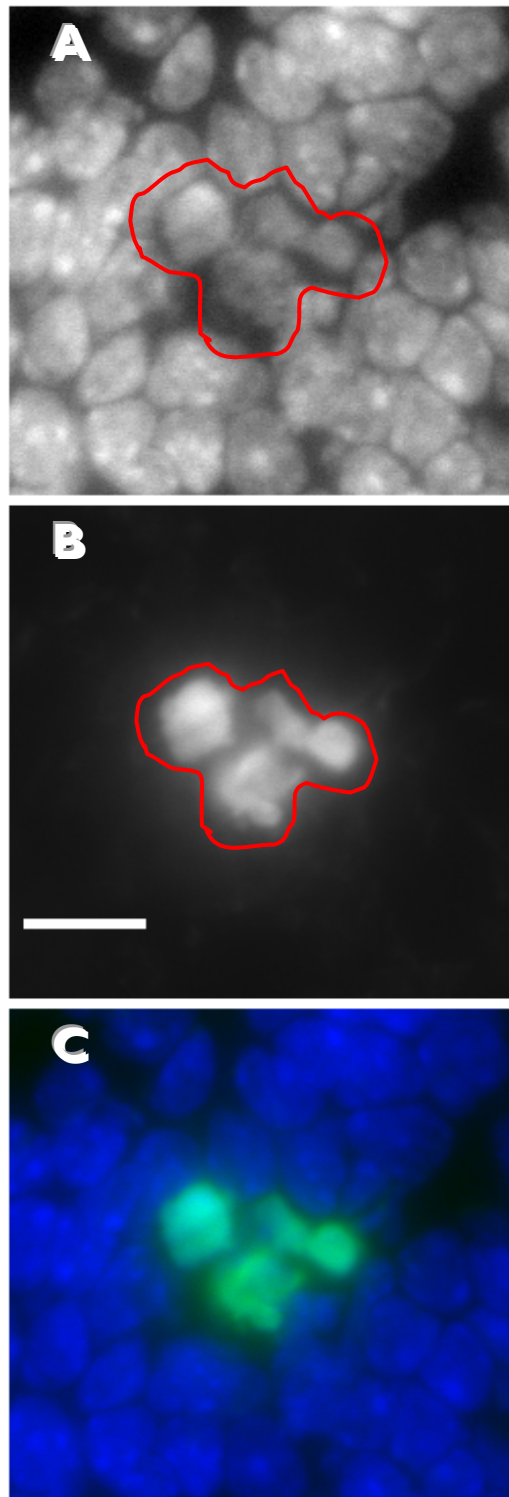


Figure 4.25: Fragmented TUNEL-stained cell nucleus

Spleen sections from recipient mice were stained for the TUNEL assay as described. Some apoptotic cells (outlined in red) showed characteristic nuclear fragmentation in both the DAPI (A) and TUNEL (B) fluorescent images. When the TUNEL-stained fragmented nucleus appeared coalesced in the pseudo-coloured composite image (C), it was counted as a single TUNEL-positive event. Images photographed with 40× objective lens, scale bar shows 10 μm .

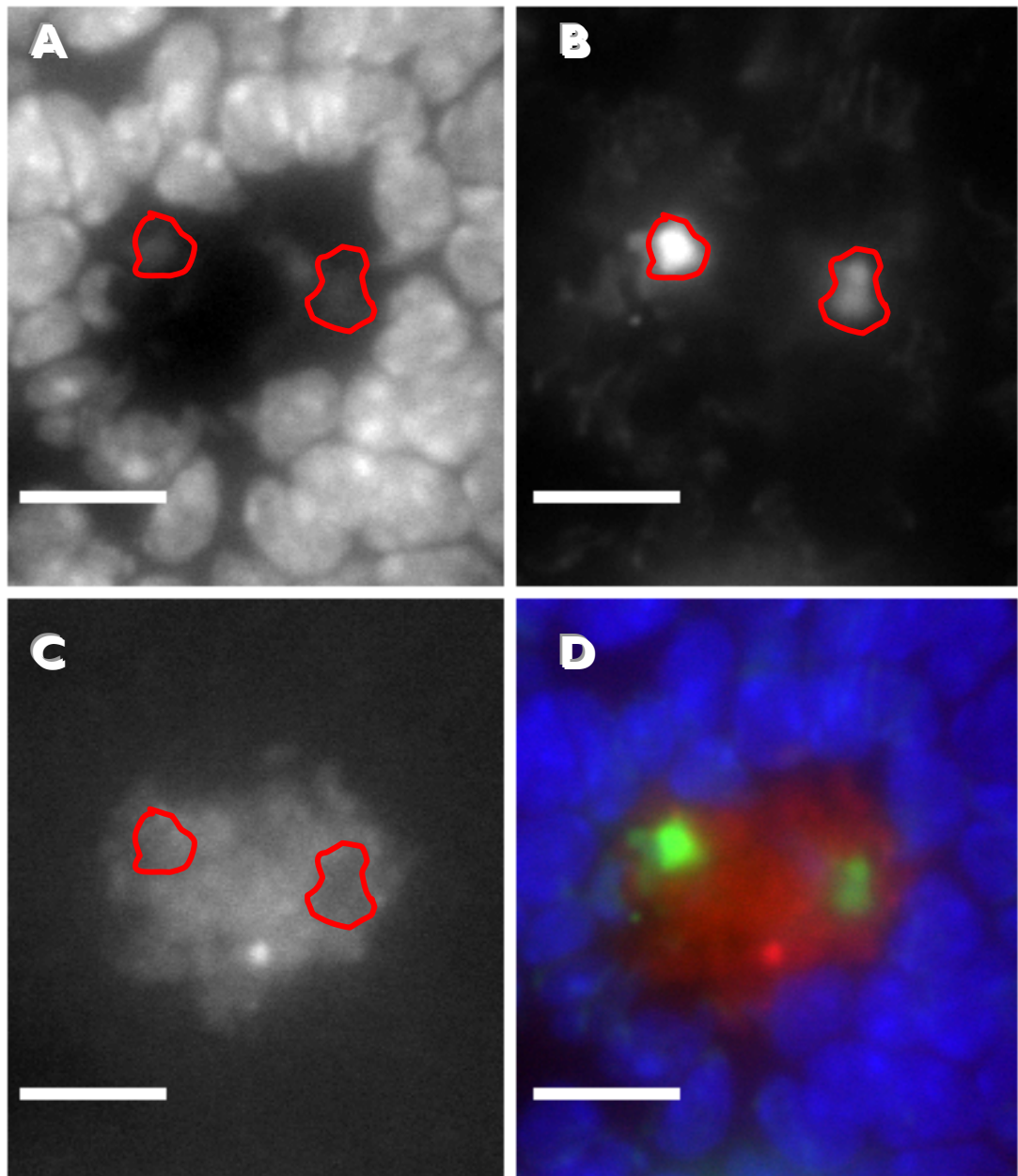


Figure 4.26: Phagocytic cell and ingested TUNEL-positive debris

Recipient spleen sections contained both lymphocytes and phagocytic cells (A) identified in the DAPI channel by their size and large cytoplasm volume (lack of DAPI-staining). Within TUNEL-stained spleen sections, TUNEL-positive material (outlined in red) was sometimes identified within these phagocytic cells (B). The presence of the phagocyte was also confirmed by the characteristic dappled autofluorescent pattern in the CMRA channel (C). When one or more TUNEL-positive particles were identified within such autofluorescent cells in the pseudo-coloured overlay (D), the event was counted as a single TUNEL-positive event. Images photographed with 40× objective lens, scale bar shows 10 μm.

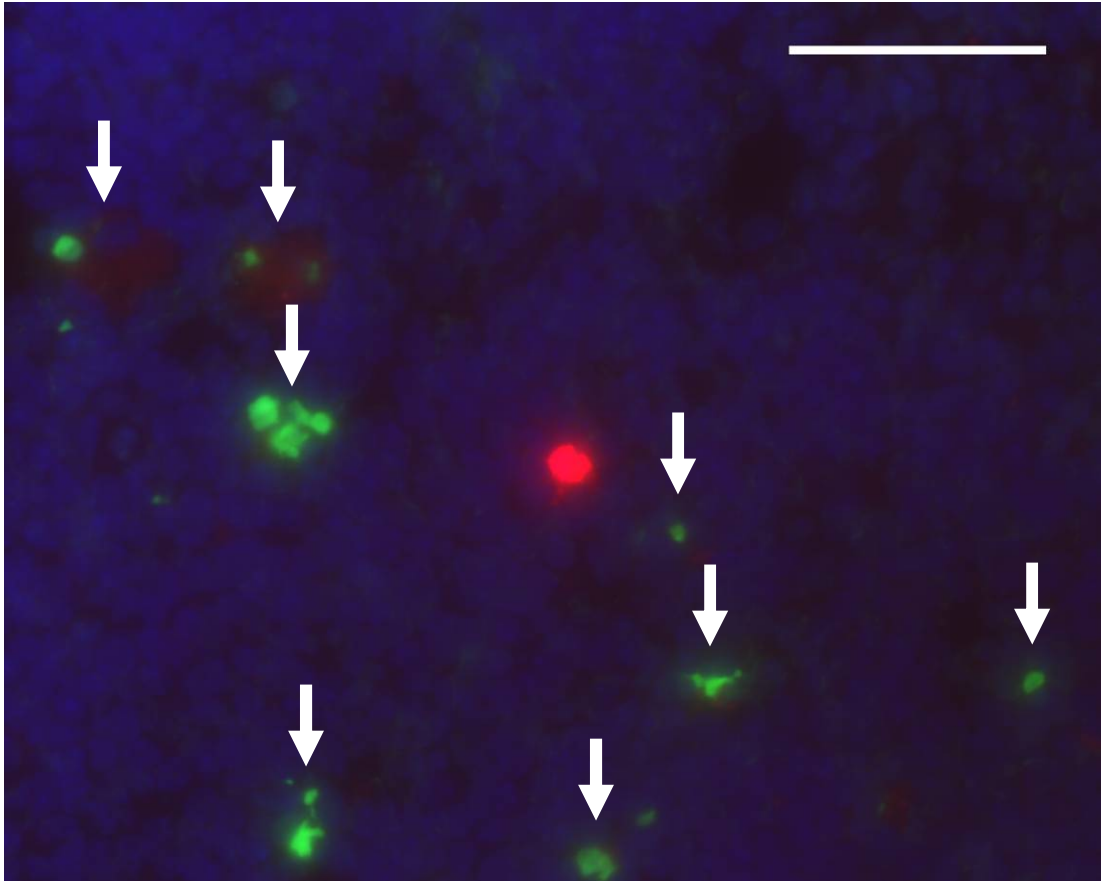


Figure 4.27: Manual apoptosis scoring in local screening field from TUNEL-stained spleen section

Spleen sections from recipient mice were stained for the TUNEL assay as described and images were recorded from the DAPI (blue), fluorescein (green) and CMRA (red) fluorescent channels for each local screening field. The images from the three fluorescent channels were overlayed to form a pseudo-coloured composite image for manual screening. TUNEL-positive events were scored manually for each field (arrowed). Scale bar shows 50 μm .

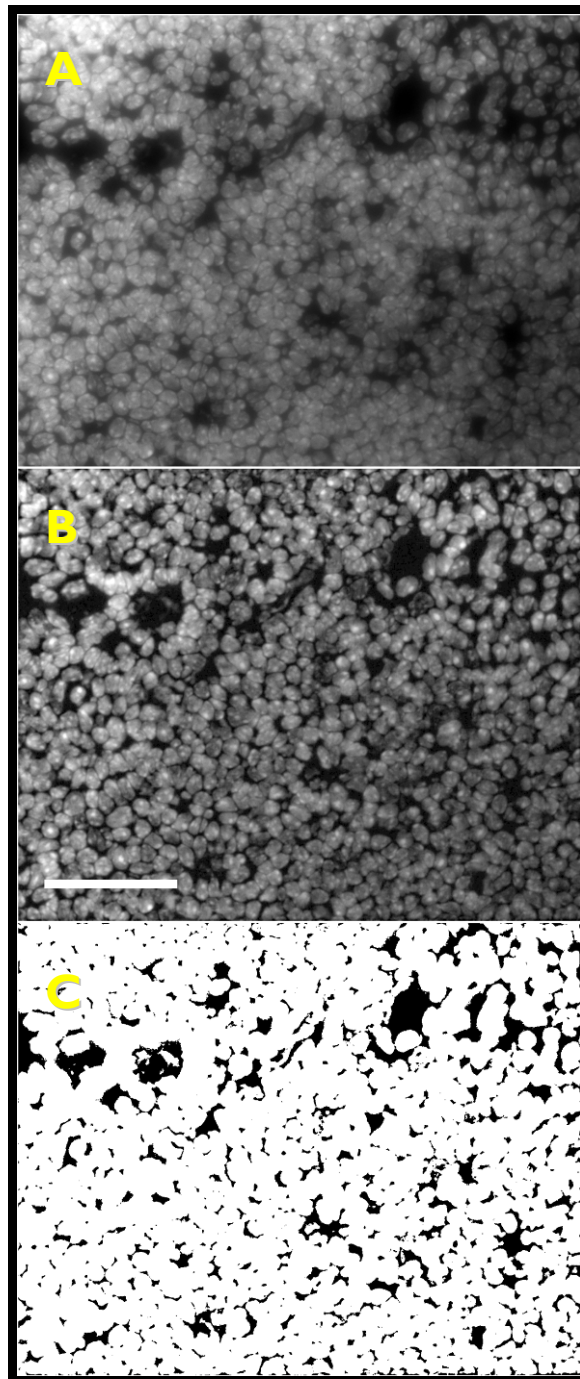


Figure 4.28: Estimating total number of cells per field

Spleen sections were counterstained with DAPI to show cell nuclei. For each field the DAPI channel image (A) was automatically processed by subtracting the background signal (50 pixel radius averaging), applying a *Smooth* filter to remove speckled pixels and applying saturation and gamma corrections to ensure even brightness across the field, resulting in an image with clear distinction between cell nuclei and unstained areas (B). A threshold brightness value was applied to binarise the processed image into stained or unstained pixels (C). The area of the field that was stained was divided by the area of a nominal cell to estimate the total number of cells in each field. Scale bar shows 50 μm .

Proliferation

Mirroring the complex death responses of irradiated cells and their unirradiated neighbours, is the proliferative capacity of the surviving cells. In measurements of surviving cell numbers, plating efficiency, clonogenicity and tumour growth, the summation of cell death and the proliferation of the survivors contributes to the observed response. As seen with cell death and apoptosis responses, whether the radiation effect is pro- or anti-proliferative depends on the dose, dose-rate, and radiation type/quality, and these effects can differ between directly irradiated and bystander cells.

Direct radiation exposure is most commonly associated with decreased proliferation (Wang *et al.*, 2004), due to the activation of checkpoint proteins (Lee *et al.*, 2006; Ponnaiya *et al.*, 2007; Short *et al.*, 2007) and subsequent cell-cycle delay (Hu and Heikka, 2000; Gerashchenko *et al.*, 2004). However, the initial decrease in proliferation may not be indicative of the outcome. Lung fibroblasts irradiated with 10 mGy of α -particles show an initial decrease in cell numbers compared to controls (24 h post-irradiation) – consistent with cell-cycle arrest – but after three days show significantly more cells compared to unirradiated controls (Iyer and Lehnert, 2000). Mice exposed to 0.5 Gy whole-body X-irradiation show increased numbers of total bone marrow cells forty-eight hours post-irradiation (Wang and Cai, 2000).

Increases in proliferation are often seen in bystander cells from irradiations with carbon ions (Shao *et al.*, 2003a), γ -rays (Gerashchenko and Howell, 2003b, 2003a, 2005) and ^3H -thymidine incorporation (Gerashchenko and Howell, 2004, 2005). As well as induction of proliferation, bystander cells have shown increased proliferative responses to subsequent mitogen-stimulation (Shankar *et al.*, 2006). Not all

bystander experiments have shown changes in proliferation (Pinto *et al.*, 2006) and some have shown different responses depending on dose, where low X-ray doses (0.075 Gy) induce, and high doses (2 Gy) depress, proliferation of co-cultured bystander cells (Liu *et al.*, 2004). *In vivo* studies have shown opposing proliferative bystander effects with radiation dose-rate (Xue *et al.*, 2002; Kishikawa *et al.*, 2006).

Choice of assay

Several methods are available for the detection of proliferating cells *in situ*, falling into two broad categories; cell-cycle-dependent label incorporation, and, the expression of cell-cycle-associated markers. The former methods require the presence of a detectable label, such as bromodeoxyuridine (or other labelled nucleoside) during an incorporation period where proliferating cells will incorporate the label into newly synthesised DNA (Gratzner, 1982). Such methods had the advantage of measuring cumulative cell division over time, but were impractical due to the need to administer the label *in vivo*, associated toxicity and that the reaction still needs to be developed by immunohistochemistry. Instead, proteins selectively expressed during certain stages of the cell-cycle can be detected in preserved tissues, but only represent a snapshot of cells that were proliferating at the moment of cryopreservation/fixation. The commonly used cell-cycle associated marker Ki-67 antigen, expressed through all stages of the cell-cycle except in quiescent cells (G₀-phase) (Endl and Gerdes, 2000; Solovei *et al.*, 2006) was chosen, since the other common alternative, proliferating cell nuclear antigen (Hall *et al.*, 1990), can be difficult to detect in frozen tissue sections (Baum *et al.*, 1994). Ki-67-positive proliferating cells within recipient spleen sections were detected using a two-step immunofluorescence method.

Method:

Frozen tissues were brought from ultra-cold storage up to -18°C prior to sectioning. Non-serial $5\ \mu\text{m}$ -thick sections were cut from the frozen embedded tissue blocks using a *Reichert-Jung Cryocut 1800* cryostat and applied to positively-charged glass microscope slides. Slides were brought to room temperature, immersed in 2% formaldehyde (from paraformaldehyde in PBS) for 20 min at room temperature, followed by washing 3×2 min in 0.1 M glycine in PBS according to the method of Erhart *et al.*, (1997). Slides were permeabilised in 1% Triton® X-100 in PBS, for 20 min at 37°C , then washed 3×2 minutes in PBS. The tissue sections were ringed with a hydrophobic barrier pen before sections were incubated with 100 μL of rabbit anti-mouse Ki-67 antibody (1/100 dilution in 1% goat serum, Lab Vision Corp., CA, USA) overnight at 4°C in a humidified slide chamber. After washing slides 3×5 minutes in PBS, slides were incubated with 100 μL goat anti-rabbit IgG–Alexa Fluor® 488 secondary antibody (1/200 dilution in PBS, Invitrogen Corp.) for 1 h at 37°C in a humidified slide chamber. Slides were washed 3×5 minutes in PBS then coverslipped with *Vectashield® with DAPI* and stored in the dark at -20°C .

Scoring method

Ki-67–staining was inspected in pseudo-coloured photographs overlaying the DAPI/nuclear counterstain (blue), *Alexa Fluor® 488*/Ki-67 staining (green) and CMRA/donor cell fluorescent probe (red) (*Figure 4.29*); however, proliferating cells were quantified by an automatic area measurement of the *Alexa Fluor® 488* fluorescence recorded in each field. Briefly, the original TIFF images taken using the *Alexa Fluor® 488* filterset were opened with the *ImageJ* software (*Figure 4.30*). Non-cell areas (without corresponding DAPI DNA-counterstain signal) showed

negligible green fluorescence. Cell nuclei co-localised with very low levels of green staining (close to background levels) or a range from moderate patterned staining to an intense even staining across the nucleus (*Figure 4.30*) (Solovei *et al.*, 2006).

An algorithm was applied to increase the contrast between the non-specific background fluorescence and the specific *Alexa Fluor*® 488 signal linked to the expression of the Ki-67 protein (*Figure 4.31*). The enhancement procedure made little difference to the intensely stained nuclei but increased the distinction between the moderately stained nuclei and the surrounding background. Following the enhancement algorithm the *ImageJ* software binarised the image at a fluorescence intensity threshold determined automatically from the difference between the background and specific staining. The proliferation index was calculated as the percentage of the field selected as Ki-67–positive divided by the percentage of the field staining positive for DAPI (as shown previously in *Figure 4.28*), for both local and global fields. The proliferation index was calculated for each spleen section as the mean index across each of the fields photographed, and for each mouse as the unweighted mean of the duplicate slides.

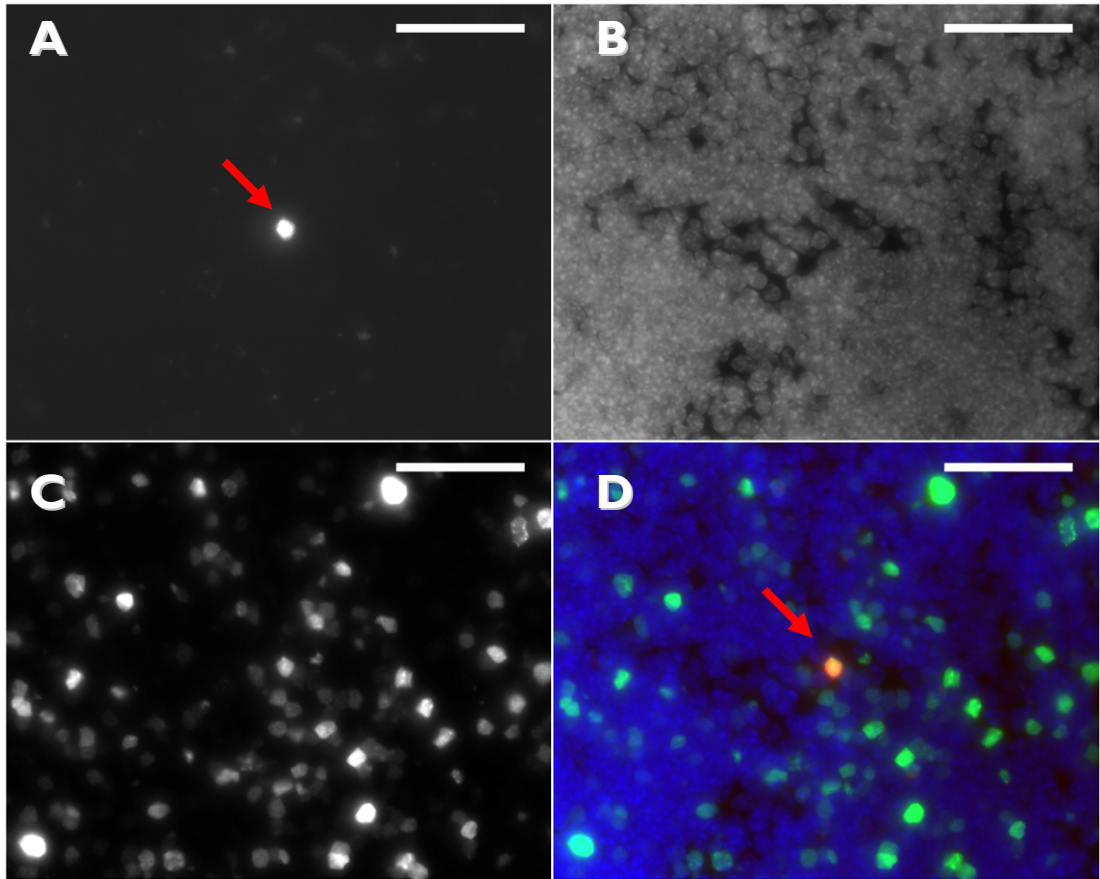


Figure 4.29: Pseudo-coloured overlay of a local screening field from Ki-67 assay

Spleen sections from recipient mice were stained for the Ki-67 assay as described. Using fluorescence microscopy, lodged donor cells were identified using the filterset for CMRA fluorescence (A) and the field of view was centred on the donor cell (arrowed, red). In the same field, cell nuclei counterstained with DAPI (B) and fluorescent Ki-67-staining (C) were photographed. The images from the three fluorescent channels, CMRA (red), DAPI (blue), and Ki-67 (green), were overlayed to form a pseudo-coloured composite image for inspection (D). The donor cell (arrowed, red) appears yellow/orange as it was also positive for Ki-67. Scale bar shows 50 μm .

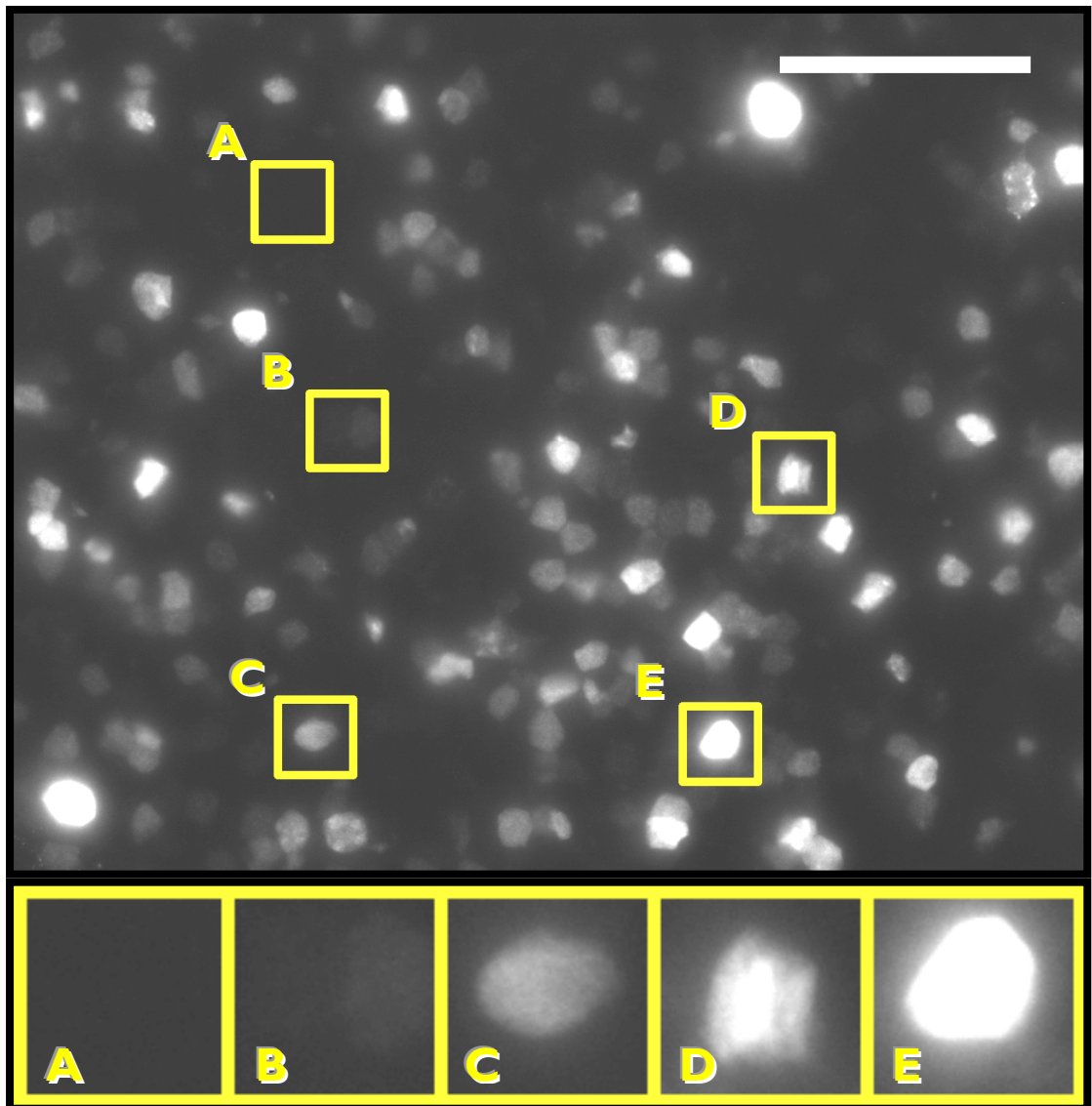


Figure 4.30: Levels of Ki-67 staining in local fields

Spleen sections from recipient mice were stained for the Ki-67 assay as described. The fluorescence on the *Alexa Fluor® 488* channel for a representative local field is shown. Scale bar shows 50 μm . Insets (15 μm \times 15 μm) are shown for a representative unstained (A), weakly stained (B), faintly stained (C), moderately stained (D) and brightly stained cell (E).

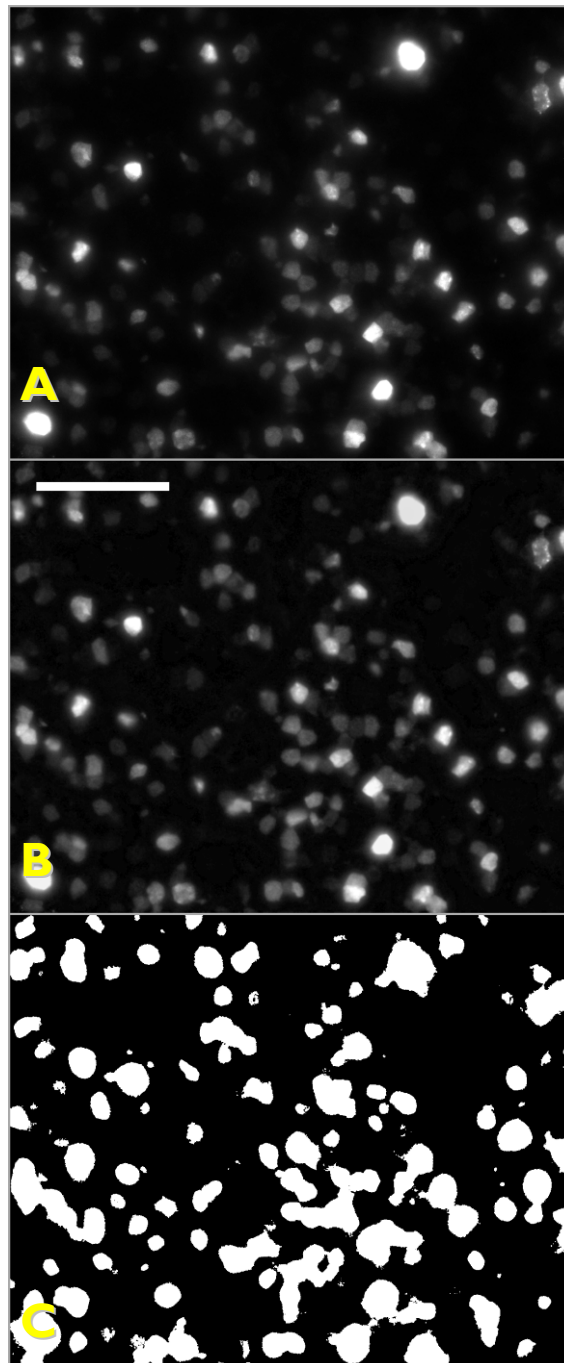


Figure 4.3 I: Automatic proliferation scoring in local screening field from Ki-67 stained spleen section

For each Ki-67 stained local field, the Ki-67 channel image (A) was automatically processed by subtracting the background signal (50 pixel radius averaging), applying a *Smooth* filter to remove speckled pixels and applying saturation and gamma corrections to ensure even brightness across the field, resulting in an image with clear distinction between Ki-67–positive cell nuclei and unstained areas (B). A threshold brightness value was applied to binarise the processed image into stained or unstained pixels (C). The percentage of the field that was Ki-67–positive was divided by the percentage of the field stained with DAPI to calculate the proliferation index. Scale bar shows 50 μm .

Chromosomal damage

The role of DNA mutations in carcinogenesis is crucial, yet the issue of causation is still under intense debate. Analysis of cancer cells clearly demonstrates the ubiquitous accumulation of DNA mutations, some deleterious, others inconsequential. However, whether the mutations were the cause of tumourigenesis or arose later due to the nature of carcinogenic cells has not yet been determined. The mutator hypothesis (reviewed in Loeb, 2001), proposes a single triggering lesion in a gene encoding a critical DNA maintenance or repair protein; this loss-of-function whilst not carcinogenic in itself, elevates the background DNA mutation-rate, increasing the risk of further carcinogenic mutations. For example, loss or mutation of a DNA methylation enzyme, resulting in incomplete or aberrant methylation patterns could trigger a cascade of DNA changes that ultimately endow tumourigenic potential on the cell. Whether an initial DNA lesion is responsible for the eventual loss of proliferative control in cancer cells or not, it is clear that DNA mutation alone is not sufficient to drive carcinogenesis. A receptive microenvironment, failure of the immune system to control aberrant cells and vascularisation are all necessary steps in the development of a tumour (reviewed in Langley and Fidler, 2007; Finn, 2008; Wels *et al.*, 2008).

Given the stochastic nature of radiation energy deposition, a direct radiation-induced lesion in a critical gene cannot alone explain the induction of cancer by radiation. Similar to the mutator hypothesis, radiation damage of DNA may instead trigger long-term changes in the regulation of DNA maintenance and repair that induces instability in the genome. This difference is particularly relevant to the issue of mutations induced in bystander cells, which do not receive radiation energy depositions. DNA mutations induced in bystander cells have been shown to be

distinct from those induced in the directly irradiated cells and more akin to DNA damage from endogenous oxidative metabolism (Huo *et al.*, 2001; Persaud *et al.*, 2005; Persaud *et al.*, 2007). DNA damage foci, thought to represent sites of DNA double-strand breaks can be induced in bystander cells, although whether these are caused directly by clastogenic factors or represent disruption of normal DNA processing is unknown (Kashino *et al.*, 2004; Hu *et al.*, 2005; Sokolov *et al.*, 2005; Hu *et al.*, 2006). Together, these uncertainties suggest that rather than short-term induction of debilitating mutations in candidate genes, the risk of bystander signalling for mutagenesis may lie in disruption or deregulation of normal DNA maintenance.

Choice of assay

The pKZ1 *in vivo* mouse chromosomal inversion assay (described on p. 52–54) detects inversions in the DNA sequence of a transgenic construct, previously shown to be induced *in vivo* by X-rays, etoposide, mitomycin C, cyclophosphamide and amifostine (Sykes *et al.*, 1998; Sykes *et al.*, 1999; Hooker *et al.*, 2002; Hooker *et al.*, 2004b; Hooker *et al.*, 2009). The ability of low doses of various agents to reduce the inversion frequency below the untreated control levels (Hooker *et al.*, 2004b; Day *et al.*, 2006; Zeng *et al.*, 2006), and the induction of inversions even by ultra-low (1–10 μ Gy) X-ray doses (Day *et al.*, 2006), suggests that inversions in the pKZ1 transgene represent more fundamental changes in the behaviour of DNA-repair and/or regulation rather than radiation-induced damage *per se*. Chromosomal inversions in pKZ1 mice have largely been studied in spleen, however, remarkably similar responses have been observed in prostatic ducts *in vivo* (Zeng *et al.*, 2006) and in a hybridoma cell line produced from a pKZ1 splenocyte (Hooker *et al.*, 2004b). DNA damage in bystander cells (if it occurs *in vivo*) is more likely to

manifest initially as changes in higher order DNA regulation: DNA methylation, chromatin structure, DNA-repair efficiency etc., which a specific mutagenesis assay might not detect as a change in any one gene. pKZ1 chromosomal inversions have proven sensitive *in vivo* to the knockout of a DNA-repair gene (Msh2), over-expression of a proto-oncogene (c-myc) and transgenic expression of a transforming oncogene (SV40 T antigen) (Hooker *et al.*, 2004a). A further advantage of this endpoint, is that the pKZ1 chromosomal inversion assay is performed entirely *in vivo*, with transgene expression analysed *in situ* in fixed tissue sections. The ability to adoptively transfer donor cells from non-transgenic littermates also allows the recipient mouse tissues to be examined without the need to discriminate between irradiated and unirradiated cells, since all transgene expression will be restricted to the bystander cells.

Method:

In experiments analysing pKZ1 chromosomal inversions, C57Bl/6J mice nullizygous for the pKZ1 transgene (pKZ1^{-/-}) were used as the donor mice and those hemizygous for the pKZ1 transgene (pKZ1^{+/-}) were used as the recipients. Frozen tissues were brought from ultra-cold storage up to -18°C prior to sectioning. Non-serial 5 µm-thick sections were cut from the frozen embedded tissue blocks using a *Reichert-Jung Cryocut 1800* cryostat and applied to positively-charged glass microscope slides. Slides were fixed in 0.25% glutaraldehyde (in 0.1 M Na₂HPO₄, pH 7.4, Sigma Aldrich Corp.) for 7 min then rinsed in 0.1 M Na₂HPO₄. X-gal stain was prepared: 0.1 M Na₂HPO₄, 5 mM K₃[Fe(CN)₆], 5 mM K₄[Fe(CN)₆]·3H₂O, 2 mM MgCl₂ and 40 mg·mL⁻¹ 5-bromo-4-chloro-3-indolyl-β-D-galactopyranoside (X-gal) in DMSO (Sigma Aldrich Corp.), and filtered (0.22 µm, Millex-GS disposable filter) to remove particulates (according to the method of Sanes *et al.*, 1986). To each spleen section, 100 µL of X-gal stain was applied and

slides were incubated for 18 h at 37°C in a humidified slide chamber. Excess stain was removed in running water before slides were air-dried and coverslips were mounted with *Aquamount* (BDH Ltd, Dorset, UK).

Scoring method

Since the pKZ1/X-gal stain is a chromogenic assay (not fluorescent), it was not compatible with the local/global screening methods using fluorescence microscopy to simultaneously view donor cells and the biological endpoint. However, since pKZ1 inversions were restricted to recipient cells (as donor cells were pKZ1^{-/-}) the assay was conducted using a modified global screening method and normal light microscopy. X-gal stained spleen sections were manually screened using a Leitz Orthoplan light microscope (Leica Microsystems GmbH) with a 40× objective lens and 8× eyepieces. Twenty random fields were selected from each spleen section and the number of cells containing bright, punctuate, blue deposits (indicative of β-galactosidase activity) was recorded (*Figure 4.32*). The total number of cells scored was estimated by multiplying the mean number of cells per unit area for that spleen by the total area screened. The pKZ1 inversion frequency was calculated as the quotient of the number of inversions detected and total cells scored. No inversions were observed in non-transgenic recipient mice screened as negative staining controls.

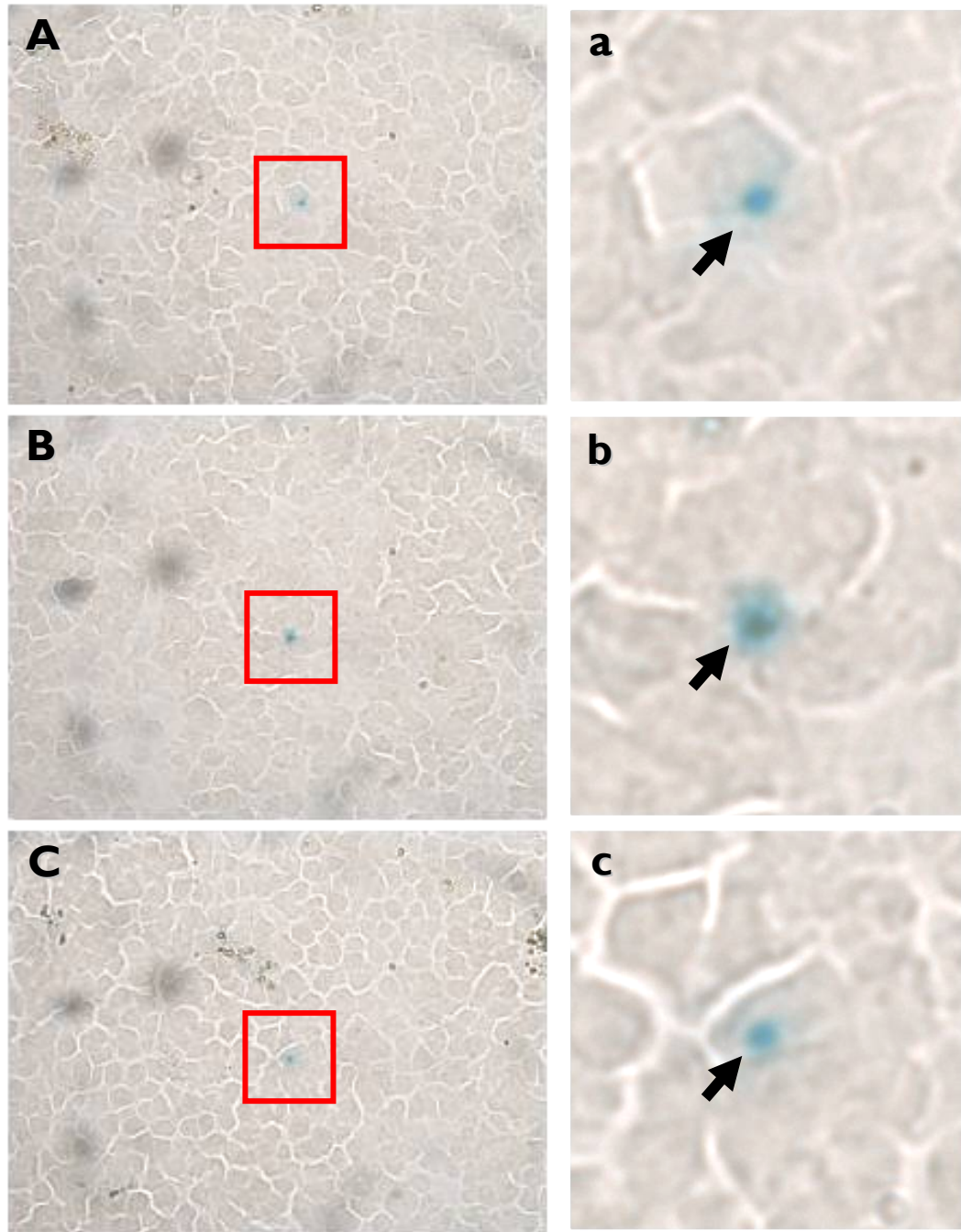


Figure 4.32: pKZI-encoded β -galactosidase activity detected in X-gal stained spleen sections

Spleen sections from pKZI^{+/-} recipient mice were stained with X-gal as described. Three different recipient cells positive for β -galactosidase activity (containing punctuate blue staining), identified by brightfield microscopy, are shown (A, B & C). The area marked by the box (red) is enlarged in the insets (a, b & c) with the blue staining indicative of pKZI inversions indicated (arrows). Non-transgenic spleens did not show any punctuate blue staining in recipient spleen cells. All donor cells were from pKZI^{-/-} mice and thus did not show any pKZI inversions.

Experimental design

Having developed and optimised the individual steps of the adoptive transfer method in mice to study radiation-induced bystander effects *in vivo*, the method was used to answer the question: ‘Do radiation-induced bystander effects of the nature seen in cell culture investigations occur *in vivo*?’ The null hypotheses tested in each experiment were as follows:

Compared to mice receiving sham-irradiated donor cells, the presence of irradiated donor splenocytes within unirradiated recipient mouse spleens will not alter:

- the frequency of apoptosis or the proliferation index, in the local area surrounding irradiated donor cells; or,
- the frequency of apoptosis, the proliferation index, or the pKZ1 inversion frequency, throughout the spleen as a whole.

If the results of an experiment supported the rejection of one or more null hypotheses, they would provide evidence for a bystander effect *in vivo*. If however, the null hypotheses were accepted, the results would uphold the assumption of no bystander effect.

A standard workflow was followed for each experiment conducted using the adoptive transfer method (*Figure 4.33*). For each experiment the specific experimental parameters were decided, the donor cells were prepared and the adoptive transfer was performed as described here. Next, the spleen tissues from the recipient mice were stained for the chosen biological assays and the biological endpoints were quantified using the two bystander screening methods. In the final phase, the data collected from the biological screens was analysed following a defined workflow (*Figure 4.34*). This data analysis protocol compared the levels of each endpoint between recipient mouse groups, assessed the variance between the two screening methods, and then checked for correlations with the donor cell levels in the fields or spleen.

To do this, each field screened was entered into a database (*SPSS 15.0 for Windows*, SPSS Inc. 2006) recording:

- the estimated total number of cells in the field;
- the raw measurements of TUNEL, Ki-67 or pKZ1 inversion staining;
- the standardised frequency for that field (e.g. number of TUNEL events in field divided by the number of cells in field);
- the number of CMRA-positive donor cells in the field; and,
- the number of CMRA-positive donor cells that showed radiolabelling by autoradiography (for local fields).

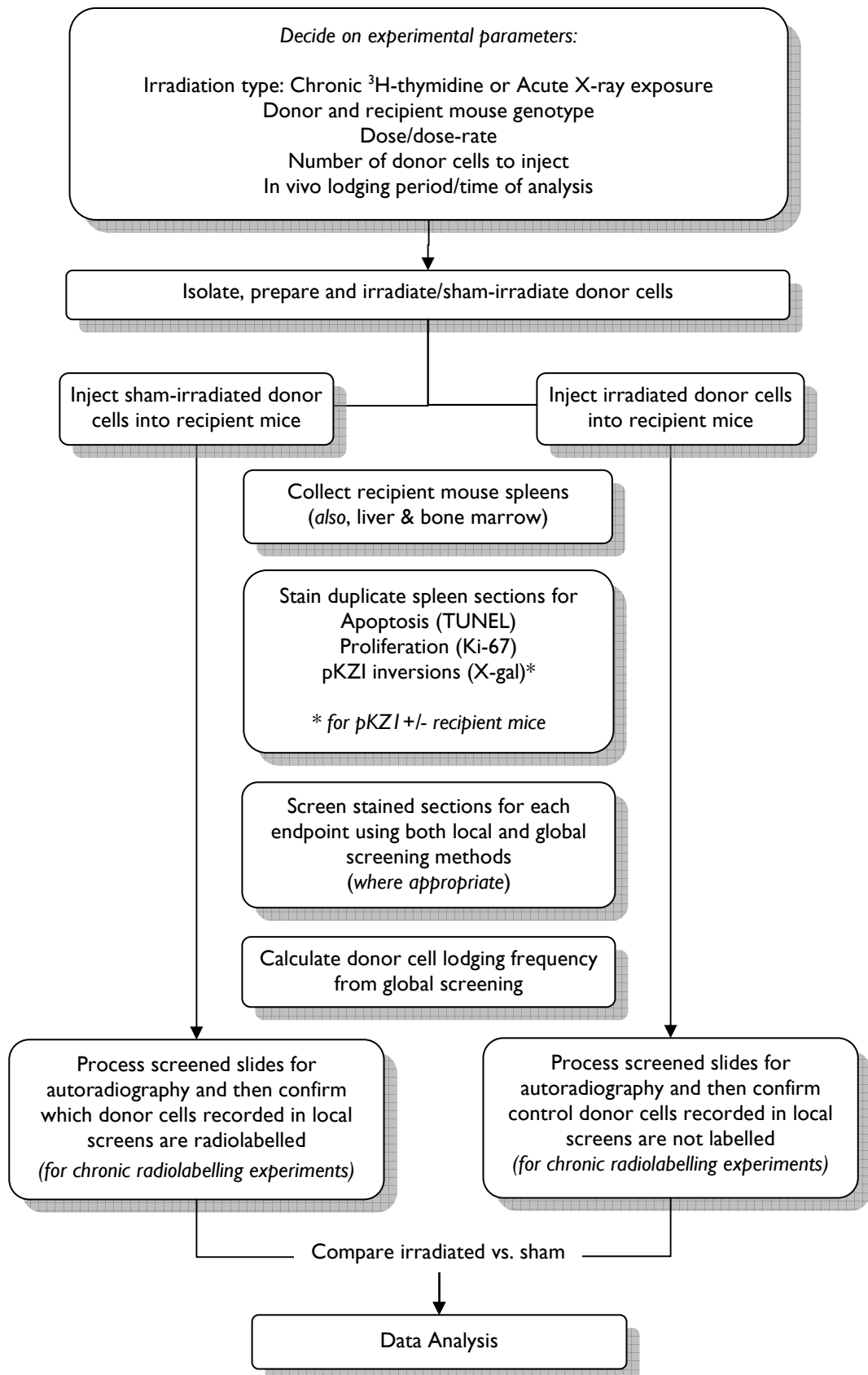


Figure 4.33: Workflow for adoptive transfer experiments

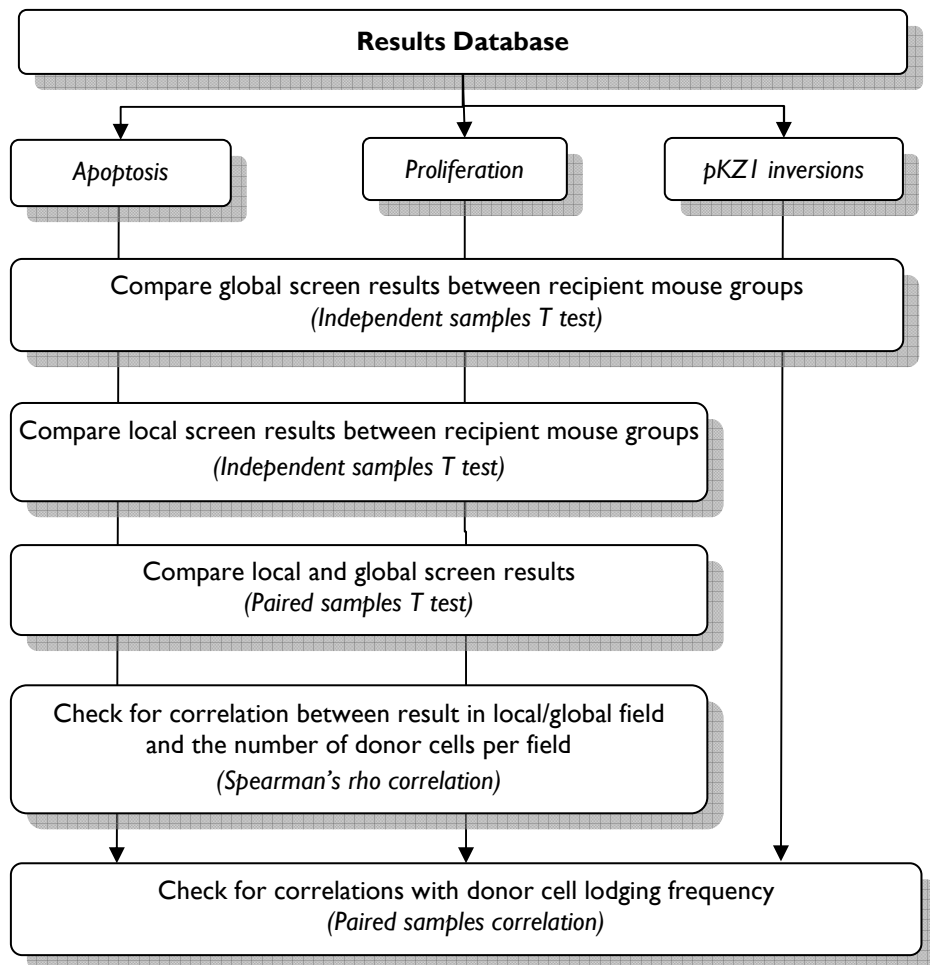


Figure 4.34: Data analysis workflow

Once data collection was complete, the slides were de-coded and the data for each field was linked to the recipient mouse and their sex, genotype, recipient mouse group, and time of injection. From these records, the data could be analysed at the level of fields, or could be grouped by mouse (mean of duplicates), treatment group, pooled by experiment, etc. to make comparisons between repeat experiments and different experimental conditions. The next chapter will now describe the use of the adoptive transfer method and the experimental strategy outlined here to explore the occurrence of radiation-induced bystander effects *in vivo*.